

Real-time 3D-aware Portrait Video Relighting

Ziqi Cai^{1,2} Kaiwen Jiang³ Shu-Yu Chen¹ Yu-Kun Lai⁴ Hongbo Fu^{5,6} Boxin Shi^{8,9} Lin Gao^{*1,7}

¹Beijing Key Laboratory of Mobile Computing and Pervasive Device, Institute of Computing Technology, Chinese Academy of Sciences

²Beijing Jiaotong University ³University of California San Diego ⁴Cardiff University ⁵City University of Hong Kong

⁶The Hong Kong University of Science and Technology ⁷University of Chinese Academy of Sciences

⁸National Key Laboratory for Multimedia Information Processing, School of Computer Science, Peking University

⁹National Engineering Research Center of Visual Technology, School of Computer Science, Peking University

{zqtsai,kevinjiangedu@gmail.com, chenshuyu@ict.ac.cn, Yukun.Lai@cs.cardiff.ac.uk
hongbofu@cityu.edu.hk, shiboxin@pku.edu.cn, gaolin@ict.ac.cn}

Abstract

Synthesizing realistic videos of talking faces under custom lighting conditions and viewing angles benefits various downstream applications like video conferencing. However, most existing relighting methods are either time-consuming or unable to adjust the viewpoints. In this paper, we present the first real-time 3D-aware method for relighting in-the-wild videos of talking faces based on Neural Radiance Fields (NeRF). Given an input portrait video, our method can synthesize talking faces under both novel views and novel lighting conditions with a photo-realistic and disentangled 3D representation. Specifically, we infer an albedo tri-plane, as well as a shading tri-plane based on a desired lighting condition for each video frame with fast dual-encoders. We also leverage a temporal consistency network to ensure smooth transitions and reduce flickering artifacts. Our method runs at 32.98 fps on consumer-level hardware and achieves state-of-the-art results in terms of reconstruction quality, lighting error, lighting instability, temporal consistency and inference speed. We demonstrate the effectiveness and interactivity of our method on various portrait videos with diverse lighting and viewing conditions.

1. Introduction

Portrait videos are widely used in various scenarios, such as video conferencing, video editing, entertainment, virtual reality, etc. However, many portrait videos are captured under unsatisfactory conditions, such as environments that are either too dark or too bright, or with virtual backgrounds that do not match the lighting of the foreground. These factors degrade the visual quality and realism of videos and affect the user experience.

Of particular significance is the context of augmented re-



Figure 1. Given a portrait video shown in the leftmost column, our method reconstructs a 3D relightable face for each video frame. Users can then adjust their viewpoints and lighting conditions interactively. The second column displays relighted video frames with a head pose yaw of 0.3, while the third column presents faces relighted under an alternative lighting condition with a frontal head pose. The rightmost column provides the predicted albedo and geometry of the reconstructed face. Please see the supplementary video for the full results.

ality (AR) and virtual reality (VR) applications, where users often seek to create 3D faces that can be dynamically relighted to fit the environment. This dynamic relighting capability becomes possible only when the underlying method is inherently 3D-aware and operates in real time.

However, 3D-aware portrait video relighting is a challenging task, since it involves modeling the complex interactions between the light, geometry, and appearance of human faces, as well as ensuring the temporal coherence and naturalness of synthesized videos. It is even more challeng-

*Corresponding author is Lin Gao

ing when real-time performance is required. Existing methods for face relighting suffer from some limitations that prevent them from being widely adopted in practice. First, most of them (*e.g.*, [31, 50, 54]) can only relight the faces from the input viewpoints, thus restricting the user’s freedom to change the camera angle or perspective. This also limits the creative possibilities and applications for AR/VR scenarios. Second, many methods (*e.g.*, [19, 56]) are designed for monocular image inputs and thus produce flickering or unnatural results when directly applied to videos, making them inferior for practical usage, where smooth and realistic transitions are expected. Third, some methods are time-consuming in terms of both training and inference. For example, ReliTalk [33] takes 3 days of training for a 2-minute video clip. Once trained, it takes 0.2 seconds to relight a video frame. Although DPR [56] achieves real-time performance, it suffers from low-quality results. It is still challenging to balance quality and efficiency with existing solutions.

In this paper, we present a novel real-time 3D-aware portrait video relighting method that jointly solves the above problems by generating realistic and consistent relighting results for faces from novel viewpoints in real time, enabling users to create realistic and natural personas for AR/VR applications, as shown in Figure 1. In summary, our technical contributions are:

- We contribute to the ongoing field of 3D-aware portrait video relighting by introducing a novel approach that achieves real-time performance while producing realistic and consistent results.
- We propose to use dual feed-forward encoders to capture the albedo and shading information within a portrait. The shading encoder is conditioned on the albedo encoder to ensure spatial alignment of albedo and shading, resulting in realistic reconstruction and accurate relighting.
- We use a novel temporal consistency network to address temporal inconsistencies in video data, reducing flickering artifacts and ensuring seamless transitions between frames.

2. Related Work

Our work closely relates to several topics, including 3D-aware portrait generation, portrait relighting, and GAN (Generative Adversarial Network) inversion.

2.1. 3D-aware Portrait Generation

3D-aware portrait generation is the task of generating realistic and diverse images of human faces. Previous work on this task relied on 3D face priors to model the geometry and appearance of faces, such as 3D morphable models [4, 25] or neural face models [14, 42]. However, these methods require expensive 3D scanning or manual annotation and often produce low-resolution or unnatural results.

With the advancement of generative models [40], it is now possible to learn a 3D representation of faces from a collection of 2D images without any explicit 3D supervision. In particular, recent approaches combine neural radiance fields (NeRF) [27] and generative models such as generative adversarial networks (GANs) [17] and diffusion models [18] to generate high-resolution and multi-view consistent face images [1, 5, 10, 28–30, 37–39, 45, 49]. In this paper, we adopt the tri-plane representation from EG3D [5] as our 3D representation for portrait synthesis and relighting. This choice is motivated by the insights presented in [20], which shows that the tri-plane 3D representation facilitates the disentanglement of albedo and shading. This disentanglement, afforded by the tri-plane structure, enables a 3D-aware approach for relighting portraits in a photorealistic manner.

2.2. Portrait Relighting

Portrait relighting requires changing the illumination of a portrait image or video while preserving the identity and appearance of the subject. Previous works (*e.g.*, [54]) used One-Light-at-A-Time (OLAT) capturing systems to obtain detailed portrait geometry and reflectance, which enabled realistic relighting results. However, OLAT data is expensive and difficult to acquire, thus limiting the applicability of these methods. To overcome this limitation, some recent works (*e.g.*, [13, 32, 50, 57]) used synthetic data for training and showed good generalization to real data.

Another line of research explored 3D-aware portrait relighting, which leveraged the recent advances in unconditional 3D-aware portrait generation [5] by combining GANs [17] and NeRFs [27]. Concurrently, Jiang *et al.* [20] and Ranjan *et al.* [35] modeled the lighting effects in generative models, either implicitly or explicitly, and achieved impressive quality of image relighting. However, these methods are unsuitable for video relighting since they require inverting each frame separately, which is time-consuming and does not ensure temporal consistency, leading to flickering artifacts.

This paper proposes a novel method for real-time 3D-aware video relighting, which builds on [20] and distills its knowledge into a feedforward network with a temporal enhancement module. Our method can produce realistic, high-quality portrait relighting videos with various lighting effects and novel views. In contrast to our approach, none of the existing portrait relighting techniques can handle consistent and real-time novel view synthesis for a video sequence.

2.3. GAN Inversion

GAN inversion aims to find a latent representation in a pre-trained model’s latent space that can reconstruct a given image with its generator. Existing GAN inversion methods can be divided into optimization-based, learning-based, and

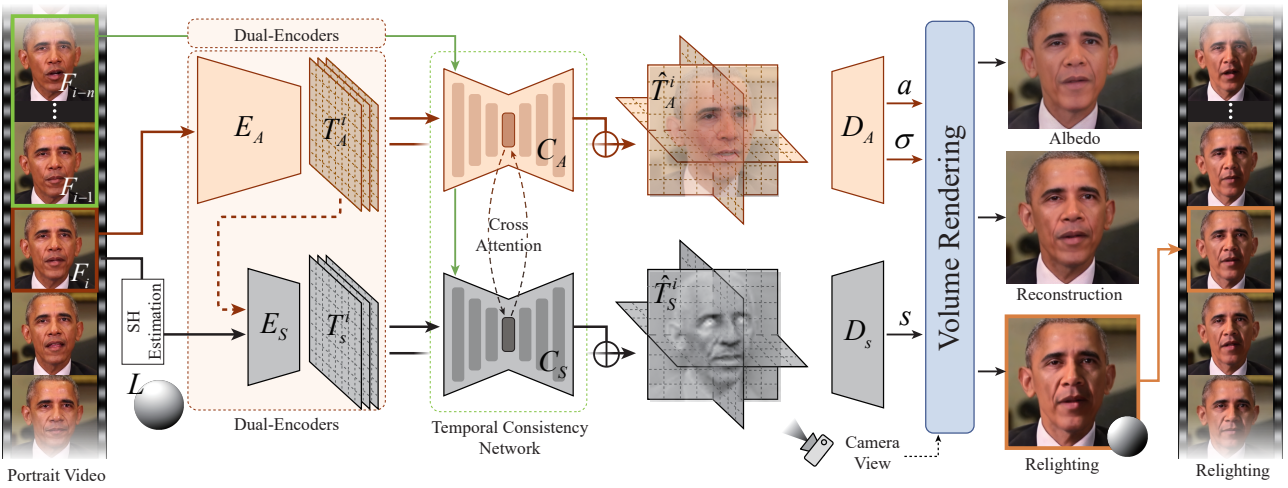


Figure 2. The pipeline of our method. Given a portrait video shown on the left side, we embed each video frame into an albedo tri-plane and a shading tri-plane using Dual-Encoders. For example, for frame F_i , we predict the albedo tri-plane T_A^i . Next, we use the estimated lighting condition L and the albedo tri-plane T_A^i to predict the shading tri-plane T_S^i that models the illumination effects on the face. Then we feed T_S^i and T_A^i along with the tri-planes predicted from previous n frames into two transformer models C_A and C_S to enhance the temporal consistency. The two transformers use cross-attention to cooperate for information sharing and alignment between the albedo and shading branches. We add the predicted residual to T_A^i and T_S^i as \hat{T}_A^i , \hat{T}_S^i for better temporal consistency. Finally, we use \hat{T}_A^i and \hat{T}_S^i to condition the volumetric rendering process, producing depth, albedo, shading, color, and super-resolved images.

hybrid approaches.

Optimization-based methods minimize reconstruction errors for high-quality results but are slow, as seen in [51] and [47], since these methods require end-to-end optimization across numerous video frames. Learning-based methods (*e.g.*, [43]), using an encoder, are faster but at the cost of lower-quality reconstruction quality. With recent trends of predicting richer information from input images, Yuan *et al.* [53], Bhattarai *et al.* [3], and Trevithick *et al.* [44] propose to predict a tri-plane from input images, striking a good balance between quality and efficiency. Hybrid methods (*e.g.*, [2, 15, 36, 52]) combine optimization and learning, enhancing both quality and efficiency. Nevertheless, their practical utility is hindered because they still require minutes to hours to process a video clip, preventing real-time applications.

Among these methods, only pure learning-based methods have the potential for real-time applications. Based on the idea of LP3D [44], we propose a novel learning-based method for video inversion, which predicts tri-plane representations from input images instead of latent codes. Tri-plane representations contain richer information than latent codes and can better capture the geometry and appearance variations of the input images. Unlike previous learning-based methods, such as [3, 43, 44, 53], that are designed for single-image inversion and thus neglect the temporal information in videos, we introduce a temporal consistency network to enforce smooth transitions between consecutive frames. Our method can achieve high-quality and consistent video inversion in real time with relighting capabilities.

3. Methodology

In this section, we give the preliminaries of the pre-trained generator in Sec. 3.1. Then, we describe how we achieve real-time video inversion and enable lighting control by using two tri-planes in Sec. 3.2. Next, we introduce how to enhance temporal consistency for video inputs in Sec. 3.3. Finally, we introduce our training objectives in Sec. 3.4. The overall pipeline is illustrated in Fig. 2.

3.1. Preliminaries

Our work distills knowledge from a pre-trained 3D-aware generator G trained based on the GAN framework [20], to enable real-time synthesis and lighting control of multiview consistent video frames. Given a latent code w in an albedo latent space, an albedo tri-plane is first predicted through a generator and then fed into a convolutional network [22] to predict a shading tri-plane, which is additionally conditioned on the second-order spherical harmonic (SH) coefficients L [34]. Both albedo tri-plane and shading tri-plane are used to condition the neural rendering process given a viewing angle. In this way, a realistic facial image I and its corresponding albedo A can be generated, while allowing the disentangled control of camera and lighting conditions.

3.2. Tri-plane Dual-encoders

We present dual-encoders (Figure 2) that can infer an albedo tri-plane and a shading tri-plane from a single RGB image. These two tri-planes are later rendered into a high-resolution (512×512) RGB image \hat{I} and an albedo image \hat{A} through a rendering process identical to [20]. Our

network extends the LP3D model [44], which encodes an image into a tri-plane representation for neural rendering. However, unlike LP3D, our network can produce two disengaged tri-planes, allowing for dynamic adjustments of lighting conditions from a single image. Our network consists of two branches: one is Albedo Encoder E_A for inferring an albedo tri-plane that captures the shape and texture of the scene, and another is Shading Encoder E_S for inferring a shading tri-plane that models the fine-grained illumination effects.

Albedo Encoder. Inspired by LP3D [44], we use an encoder based on Vision Transformer (ViT) [12] in the albedo branch for albedo prediction. The input to our method is a single RGB image F with an overlaid coordinate map, forming a 5-channel image. We used a DeepLabV3 [7] network pretrained on ImageNet [8] to extract low-frequency features from the input image, which capture global context and semantic information. We then feed these features into a ViT-based encoder [44] that further enhances the global features by self-attention mechanisms to get final low-frequency feature f_{low} . We also use a convolutional neural network (CNN) [44] to extract high-frequency features f_{high} from the input image F , which capture the fine details and edges. We feed f_{high} into another ViT-based encoder [44], along with the low-frequency features f_{low} to predict the final albedo tri-plane T_A .

Shading Encoder. To predict the shading tri-plane T_S , we use a CNN with additional StyleGAN [22] blocks, conditioned on the albedo tri-plane T_A and the lighting condition L . We represent the lighting condition L as second-order SH coefficients mapped using an off-the-shelf mapping network [20]. This design ensures that the shading tri-plane T_S are spatially aligned with the albedo tri-plane T_A for realistic reconstruction and relighting.

We employ a three-stage training strategy for our encoder. In the initial stage, we adhere to the procedure outlined in [44] to train the albedo encoder, focusing on reconstructing the provided portrait without considering the disentanglement between albedo and shading. In the second stage, we independently train the albedo branch and the shading branch. In the third stage, we integrate the two branches and train them jointly. This strategic approach enhances convergence and performance compared to training both branches simultaneously from the outset.

3.3. Temporal Consistency Network

We aim to invert a video sequence into a sequence of tri-planes, which are low-dimensional representations of the 3D scene structure, texture, and illumination. However, simply inverting each video frame independently leads to temporal inconsistency and causes flickering artifacts in the rendered images.

To address this problem, we propose a temporal consistency

network (Figure 2), which exploits the rich temporal information in the video sequence to enhance the temporal consistency of the tri-plane features. The network is composed of two transformers, denoted as C_A and C_S , accompanied by an additional convolutional neural network (CNN). Our design is inspired by [24], yet distinctively employs features at the tri-plane level. Both transformers take in corresponding predicted tri-planes for n frames, and predict residual tri-planes for each frame i to be added to the original tri-planes as \hat{T}_A^i, \hat{T}_S^i . The residual tri-planes capture the temporal variations and dynamics of the subject and help to eliminate the flickering effects. Moreover, this network uses cross-attention between the albedo branch and the shading branch, which allows them to interact with each other for better temporal consistency.

We use synthetic data to train such a temporal consistency network. Similar to training the tri-plane encoder, we generate synthetic data with augmentation techniques tailored for temporal consistency. This involves interpolating between two randomly selected camera views to simulate realistic video sequences. Additionally, random noise is added to both tri-planes to emulate flickering effects. This process for generating synthetic data provides us with a ground truth for de-flickering, devoid of errors stemming from inaccurate camera and lighting estimations. We empirically find that such a temporal consistency network trained on dynamic viewing angles and artificial noises make our method robust towards more diverse temporal dynamics in the real-world case, such as dynamic expressions.

3.4. Training Objectives

We first train our tri-plane dual-encoders to converge, and then train the temporal consistency network. Specifically, the tri-plane dual-encoders are trained with loss defined as follows:

Albedo Loss. This loss quantifies the dissimilarity between the predicted and ground-truth albedo images and tri-planes. Specifically, the albedo loss is defined as:

$$\mathcal{L}_{\text{albedo}} = \|\hat{A} - A\|_1 + \|\hat{A}_r - A_r\|_1 + \mathcal{L}_{\text{lpips}}(\hat{A}, A) + \mathcal{L}_{\text{lpips}}(\hat{A}_r, A_r) + \lambda_g \|\hat{T}_g - T_g\|_1, \quad (1)$$

where $\mathcal{L}_{\text{lpips}}$ denotes a perceptual loss [55], \hat{A}_r , \hat{A} , and \hat{T}_g are the rendered albedo images in the raw and super-resolution domains, and the predicted albedo tri-plane, respectively. A , A_r , and T_g are the corresponding ground truth. The parameter λ_g decreases from 1 to 0.01 after the initial 8 million iterations.

Shading Loss. This loss measures the disparity between the predicted and ground-truth shading features. It is defined as

$$\mathcal{L}_{\text{shading}} = \|\hat{S} - S\|_1 + \lambda_s \|\hat{T}_S - T_S\|_1, \quad (2)$$

where \hat{S} and \hat{T}_S are the predicted shading maps and the shading tri-plane, respectively, and S and T_S are the corre-

sponding ground truth. The parameter λ_s decreases from 1 to 0.01 after the initial 8 million iterations.

RGB Loss. This loss assesses the dissimilarity between the predicted and ground-truth composed images in the raw, super-resolution, and feature domains. In addition to a perceptual loss [55], an identity loss [9] is employed to retain the appearance and identity of facial images. The RGB loss is defined as

$$\mathcal{L}_{\text{rgb}} = \|\hat{I} - I\|_1 + \|\hat{I}_r - I_r\|_1 + \mathcal{L}_{\text{lpips}}(\hat{I}, I) + \mathcal{L}_{\text{lpips}}(\hat{I}_r, I_r) + \lambda_f \|\hat{I}_f - I_f\|_1 + \mathcal{L}_{\text{id}}(\hat{I}, I), \quad (3)$$

where \hat{I} , \hat{I}_r , and \hat{I}_f are the predicted RGB images in the raw, super-resolution, and feature domains, respectively, and I , I_r , and I_f are the corresponding ground truth. The parameter λ_f decreases from 1 to 0 after the initial 8 million iterations.

Adversarial Loss. This loss enforces the indistinguishability of the predicted RGB images from the source RGB images in both the raw and super-resolution domains. A dual discriminator D from [20] is utilized to discriminate between the predicted and real images. The adversarial loss is defined as

$$\mathcal{L}_{\text{adv}} = -(\mathbb{E}[\log D(I)] + \mathbb{E}[\log D(I_r)] + \mathbb{E}[\log(1 - D(\hat{I}))] + \mathbb{E}[\log(1 - D(\hat{I}_r))]). \quad (4)$$

Our final loss function for training the dual-encoders is the weighted sum of the above losses:

$$\mathcal{L} = \lambda_{\text{albedo}} \mathcal{L}_{\text{albedo}} + \lambda_{\text{shading}} \mathcal{L}_{\text{shading}} + \lambda_{\text{rgb}} \mathcal{L}_{\text{rgb}} + \lambda_{\text{adv}} \mathcal{L}_{\text{adv}}, \quad (5)$$

where λ_{albedo} , λ_{shading} , λ_{rgb} and λ_{adv} are the weights for each loss term. Initially, we set $\lambda_{\text{albedo}} = \lambda_{\text{shading}} = \lambda_{\text{rgb}} = 1$ and $\lambda_{\text{adv}} = 0$. After the first 16M iterations, we activate the adversarial loss by setting $\lambda_{\text{adv}} = 1$ and keep the other weights unchanged.

For training our temporal consistency network, besides a reconstruction loss, we use an additional temporal loss similar to [6, 24] to ensure consistency in both short-term and long-term contexts. Specifically, this loss is defined as follows:

Temporal Consistency Loss. Without losing generality, we assume current frame index is i for discussion. The short-term temporal loss is computed by calculating the optical flow f_s between consecutive input frames F_i and F_{i-1} . Subsequently, the previous outputs are warped to align with the current frame. Formally, the short-term temporal loss is defined as:

$$\mathcal{L}_{\text{short}} = M_s^i \sum_{\omega \in \{\hat{I}, \hat{I}_r, \hat{A}, \hat{A}_r, \hat{S}\}} \mathcal{L}_{\text{lpips}}(\omega^i - \tilde{\omega}^{i-1}), \quad (6)$$

where \hat{I}^i , \hat{I}_r^i , \hat{A}^i , \hat{A}_r^i , and \hat{S}^i represent the currently predicted RGB image, raw RGB image, albedo image, raw albedo image, and shading image, based on the summation of original tri-planes and predicted residual tri-planes, respectively. Similarly, \tilde{I}^{i-1} , \tilde{I}_r^{i-1} , \tilde{A}^{i-1} , \tilde{A}_r^{i-1} , and \tilde{S}^{i-1} are the corresponding frames warped using f_s from the

previous time step. The mask M_s^i is defined as $M_s^i = \exp(\|I^i - \tilde{I}^{i-1}\|_1)$, which mitigates errors introduced during the warping process.

For the long-term temporal loss, the same procedure is applied, but with the temporal index $i - 1$ replaced by 1. In other words, this process ensures temporal consistency between the first frame and the current frame. Similarly, the long-term temporal loss is defined as

$$\mathcal{L}_{\text{long}} = M_l^i \sum_{\omega \in \{\hat{I}, \hat{I}_r, \hat{A}, \hat{A}_r, \hat{S}\}} \mathcal{L}_{\text{lpips}}(\omega^i - \tilde{\omega}^1), \quad (7)$$

where \tilde{I}^{i-1} , \tilde{I}_r^{i-1} , \tilde{A}^{i-1} , \tilde{A}_r^{i-1} , and \tilde{S}^{i-1} are the corresponding frames warped using f_l from the first time step. The mask M_l^i is defined as $M_l^i = \exp(\|I^i - \tilde{I}^1\|_1)$.

Our final loss function for training the temporal consistency network is

$$\mathcal{L}_{\text{temporal}} = \lambda_{\text{short}} \mathcal{L}_{\text{short}} + \lambda_{\text{long}} \mathcal{L}_{\text{long}} + \lambda_{\text{lpips}} \mathcal{L}_{\text{lpips}}(\hat{I}^i, I^i). \quad (8)$$

where I^i denotes the ground-truth image, $\mathcal{L}_{\text{lpips}}$ promotes the reconstruction and $\lambda_{\text{short}} = 1$, $\lambda_{\text{long}} = 1$, $\lambda_{\text{lpips}} = 1$.

4. Experiments

In this section, we show our experimental setup and discuss the results of our experiments. The comparisons with alternative methods, and ablation study show the effectiveness of our method and its superiority to the alternative approaches.

4.1. Implementation Details

Datasets. We evaluate our method on the portrait videos from INSTA [58], which consist of 31,079 frames in total. Following [48], we crop the images and videos to focus on the faces. We estimate the camera pose for each frame using the technique from [5]. We also extract the lighting conditions with DPR [56].

Training Details. As to the tri-plane dual-encoders, we first freeze the generator and train only our encoder. After the first 16M iterations, we unfreeze the albedo decoder, shading decoder, and super-resolution module and train them jointly with the dual-encoders. As to the temporal consistency network, we sample camera poses from normal and uniform distributions for each person. We use two views for each person. For the first view, we sample the focal length, camera radius, principal point, camera pitch, camera yaw, and camera roll from $N(18.837, 1)$, $N(2.7, 0.1)$, $N(256, 14)$, $U(-26^\circ, 26^\circ)$, $U(-49^\circ, 49^\circ)$, and $N(0, 2^\circ)$, respectively. For the second view, we sample the camera pitch and camera yaw from $U(-26^\circ, 26^\circ)$ and $U(-36^\circ, 36^\circ)$, respectively and fix the other parameters to 18.837 (focal length), 2.7 (camera radius), 256 (principal point), and 0 (camera roll).

We train our network using the Adam [23] optimizer with a learning rate of 0.0001, except for the Transformer parameters, which have a learning rate of 0.00005. It takes about 30 days to train our network on 8 NVIDIA Tesla

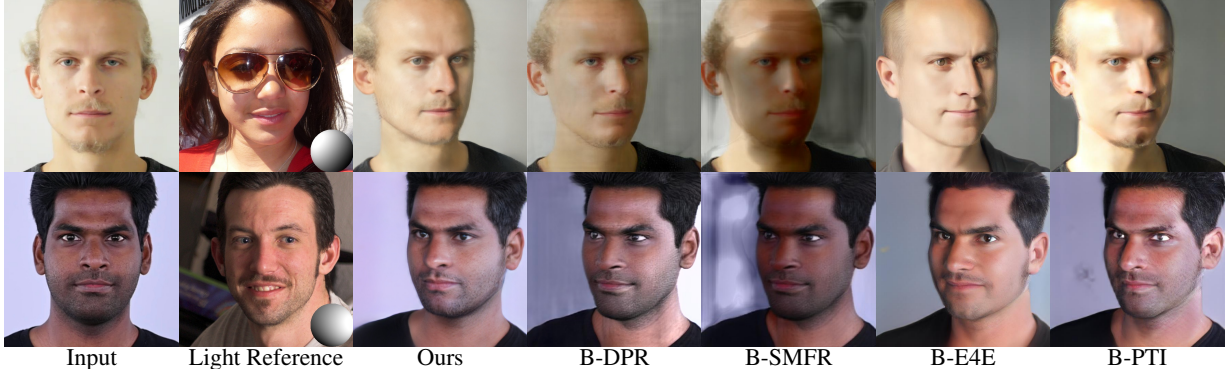


Figure 3. Comparison of video relighting quality on novel views. Our method produces more realistic and consistent results than the baseline methods introduced in Sec. 4.2.



Figure 4. Comparison of video relighting quality in the input view. We compare our method with three methods: SMFR [19], DPR [56], and ReliTalk [33]. We show the input video frames in the first row and the relighted results under different lighting conditions in the remaining rows. Our method produces more realistic and consistent results than other methods, especially under challenging conditions like the side lighting.

V100 GPUs with batch size 32. More details can be found in the supplementary material.

Inference Speed. We employ a single RTX 4090 GPU during inference. The average inference time for each frame is 30.32 milliseconds, resulting in an average of 32.98 frames per second (fps), excluding secondary tasks such as

image I/O and data transfer between the CPU and GPU.

4.2. Quantitative Evaluation

To evaluate the performance of our method, we compare it with other methods capable of 3D-aware portrait relighting. However, none existing techniques can achieve this goal in a single step, so we have to combine different methods to construct the baselines. Specifically, we use the following methods. **B-DPR** uses PTI [36] to invert each frame of an input video as a latent code of EG3D [5], allowing for rendering novel views and relighting using DPR [56]. **B-SMFR** uses the same inversion and rendering method as B-DPR, but uses SMFR [19] to relight the rendered frames from novel views. **B-E4E** uses an off-the-shelf encoder from a state-of-the-art NeRF-based face image relighting method [20] to invert each frame of the input video and relight it from novel views, which achieves real-time performance at the cost of quality. **B-PTI** uses the same encoder as B-E4E, but we apply the PTI [36] to fine-tune a single generator for each input video. This improves the reconstruction quality but takes more training time than B-E4E. We evaluate the performance of different methods regarding reconstruction quality, novel view relighting quality, identity perseverance, and time cost.

Novel View Relighting Quality. To evaluate the relighting quality under novel views, we relight first 500 frames from each video from [58]. We render each video from three novel views and pair them with five distinct lighting conditions, resulting in a total of 75,000 frames for a comprehensive comparison. Following [20], we adopt an off-the-shelf estimator [14] to calculate the lighting accuracy and instability. We use MagFace [26], different from the one we use in training, to measure identity preservation between different views. To assess temporal consistency, we use an optical flow estimator [41] to calculate warping error (WE). This involves warping the preceding frame to align with the current frame and measuring MSE loss. We also compute the LPIPS between adjacent frames for an additional evaluation of temporal consistency. We list the time

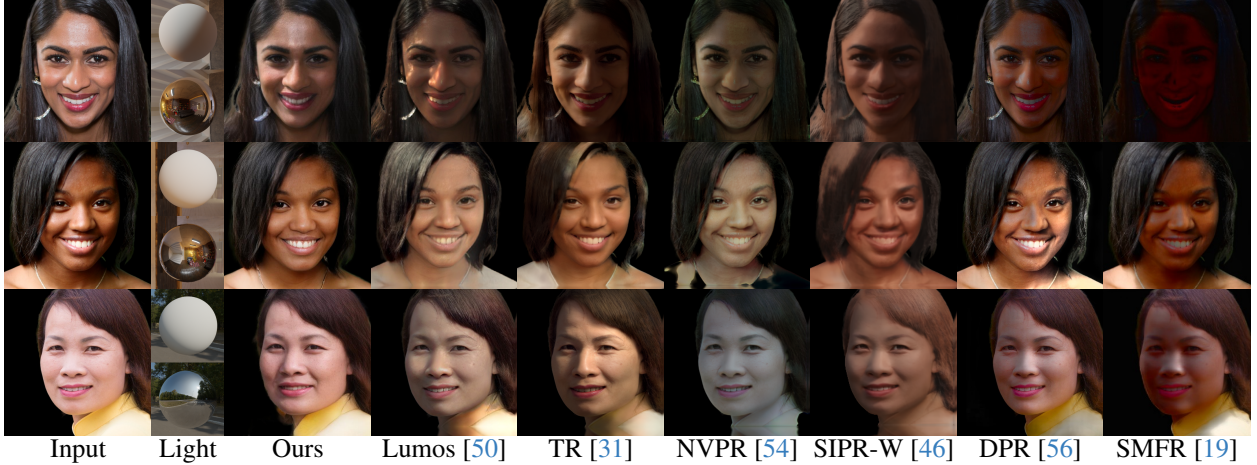


Figure 5. Comparison of relighting quality on the input view. We compare our method with six methods: Lumos [50], TR [31], NVPR [54], SIPR-W [46], DPR [56] and SMFR [19]. We show the input image in the first column, the sphere renderings from the environment map in the second column, and the relighted results in the remaining columns. Our method produces more realistic and consistent results than the other methods.

Table 1. Quantitative evaluation using lighting error (LE), lighting instability (LI), Identity Perservance (ID), Warping Error (WE), LPIPS between consecutive frames and avarage time cost (Time) on the INSTA [58] video dataset. We highlight the best score in boldface and underline the second best.

	LE \downarrow	LI \downarrow	ID \uparrow	WE \downarrow	LPIPS \downarrow	Time (s) \downarrow
B-DPR	0.9093	0.3041	0.5222	0.0029	0.1015	200
B-SMFR	1.0929	0.3352	<u>0.4479</u>	0.0022	0.0626	200
B-E4E	0.6384	0.1963	0.2892	<u>0.0007</u>	<u>0.0306</u>	<u>0.2</u>
B-PTI	0.8220	0.2630	0.4728	0.0049	0.1080	30
Ours	<u>0.7710</u>	<u>0.2533</u>	0.5396	0.0003	0.0159	0.03

each method takes to relight a face. Table 1 summarizes the quantitative evaluation results using the lighting error, lighting instability calculated based on the lighting transfer task introduced in [20], identity preservation (ID), and processing time (Time) on the INSTA [58] video dataset. Our method outperforms the baselines, demonstrating the second lowest lighting error and instability, the highest identity preservation, the lowest warping error and LPIPS, and the lowest time cost.

Reconstruction Quality. To assess the quality of reconstruction, we use four quantitative metrics: LPIPS [55], DISTs [11], Pose Error (Pose), and Identity Preservation (ID). We obtained and used the same test data as LP3D [44].

Input View Relighting Quality. We compare our method with four state-of-the-art portrait relighting methods: SIPR-W [46], TR [31], NVPR [54], and Lumos [50]. We follow the same protocol as Lumos to obtain the results for comparison. As shown in Table 3, our method achieves the lowest Fréchet Inception Distance, suggesting more realistic outcomes, and the highest Identity Preservation. For a visual comparison, please refer to Figure 4, where our approach yields the most realistic and natural results.

For the video input, we evaluate the relighting accuracy and instability while performing the video relighting on the

Table 2. Quantitative evaluation using LPIPS, DISTs, Pose Accuracy (Pose), and Identity Consistency (ID) on 500 FFHQ images. \dagger Evaluated only using the face region. \ddagger Evaluated only using the foreground on 256^2 images. We highlight the best score in boldface and underline the second best.

	LPIPS \downarrow	DISTS \downarrow	Pose \downarrow	ID \uparrow
HeadNeRF \dagger	.2502	.2427	.0644	.2031
LP3D \dagger	.1240	.0770	<u>.0490</u>	.5481
Ours \dagger	<u>.1746</u>	<u>.1134</u>	.0323	.7109
ROME \ddagger	.1158	.1058	.0637	.3231
LP3D \ddagger	.0468	.0407	<u>.0486</u>	<u>.5410</u>
Ours \ddagger	<u>.1053</u>	<u>.0835</u>	.0327	.7201
EG3D-PTI	.3236	.1277	.0575	.4650
LP3D	.2692	.0904	.0485	.5426
LP3D(LT)	.2750	<u>.1021</u>	.0448	.5404
NFL-PTI	.2332	.1627	.0228	.6825
Ours	<u>.2400</u>	.1282	<u>.0365</u>	.7015

Table 3. Quantitative evaluation on the cropped test set of FFHQ [21]. We highlight the best score in boldface and underline the second best.

	SIPR-W	NVPR	TR	Lumos	SMFR	Ours
FID \downarrow	87.39	65.23	55.30	55.18	51.16	45.08
ID \uparrow	0.6442	0.7242	0.6193	<u>0.7374</u>	0.6285	0.7711

input view. Following [20], we adopt an off-the-shelf estimator [14], which is different from the one [56] we use during the inference time, to calculate the lighting accuracy and the lighting instability. As shown in Table 4. Compared to DPR, SMFR and ReliTalk, our method achieves the lowest lighting instability and the second lowest lighting error.

4.3. Qualitative Evaluation

We conduct a qualitative evaluation on portrait videos from [16] to demonstrate the effectiveness of our method.

Novel View Relighting Quality. Figure 3 shows our method’s novel view synthesis capability under various viewpoints and lighting conditions. Among the five meth-

Table 4. Quantitative evaluation using the lighting error, lighting instability, and average time cost (Time) on the INSTA [58] video dataset. We highlight the best score in boldface and underline the second best.

	Lighting Error \downarrow	Lighting Instability \downarrow	Time (s) \downarrow
DPR [56]	0.7600	0.2997	0.04
SMFR [19]	1.1381	0.2895	0.06
ReliTALK [33] †	1.2012	0.4060	0.20
Ours	<u>0.7816</u>	0.2841	0.03

Table 5. Ablation study on temporal consistency network. We removed the temporal consistency network and calculate Lighting Error (LE), Lighting Instability (LI), Warping Error (WE) and LPIPS between consecutive frames. We highlight the best score in boldface.

	LE \downarrow	LI \downarrow	WE \downarrow	LPIPS \downarrow
w/o TCN	0.7707	0.2526	0.0006	0.0304
Ours	0.7710	0.2533	0.0003	0.0159

ods, our method preserves the lighting conditions of the reference images the most faithfully.

Input View Relighting Quality. Figure 4 presents the video relighting results in the input view by our method in comparison with three existing methods. Our approach demonstrates superior accuracy in reproducing lighting effects, especially compared to existing non-3D-aware methods. This is particularly evident under challenging lighting conditions, such as side lighting, where our method outperforms others in maintaining image quality.

4.4. Ablation Study

We perform an ablation study to evaluate the necessity of each key component in our method.

Temporal Consistency Network. We remove the temporal consistency network and then compute lighting error and lighting instability based on the lighting transfer task introduced in [20]. We also evaluate the temporal consistency based on the warp loss and LPIPS loss between consecutive frames, which serve as a reliable approximation of human perception regarding temporal consistency, capturing nuances like flickering effects. As shown in Table 5, the absence of the temporal consistency network results in an increase in warping error and LPIPS, signaling a decline in temporal consistency.

Tri-plane Dual-Encoders Design. We remove the dual-encoders (DE) and use an existing latent code encoder from [20] instead. While this alternative design does achieve real-time 3D-aware relighting, it comes at the cost of a substantial reduction in reconstruction quality, as visually depicted in Figure 6.

5. Conclusion, Limitations and Future Work

Conclusion. We introduced a real-time 3D-aware method for portrait video relighting and novel view synthesis. Our method can recover coherent and consistent geometry and



Figure 6. Albtion study comparing our model with and without the tri-plane encoders. The model without tri-plane encoders replaces our tri-plane encoders with an existing latent space encoder. This replacement results in images that bear much less resemblance to the input person, indicating a lower level of identity preservation.

relight the video under novel lighting conditions for a given facial video. Our method combines the benefits of a relightable generative model, *i.e.*, disentanglement and controllability, to capture the intrinsic geometry and appearance of the face in a video and generate realistic and consistent videos under novel lighting conditions. We evaluated our method on portrait videos and showed its superiority over existing methods in terms of lighting accuracy and lighting stability. Our work opens up new possibilities for 3D-aware portrait video relighting and synthesis.

Limitations. One of the limitations of our method is that it fails to model glares on the eyeglasses, as shown in the rightmost column of Figure 4. Future enhancements could benefit from incorporating advanced reflection and refraction modeling techniques. Furthermore, our method does not separate the motion information from the identity information, thus limiting its ability to perform video-driven animation. This challenge might be addressed through the integration of the latest advancements in talking head generation techniques.

Future Work. We are interested in extending our method to handle more complex scenes, such as multiple faces, occlusions, and full-body relighting. We also intend to explore more applications of our method, such as face editing and animation.

Acknowledgement

This work was supported by National Natural Science Foundation of China (No. 62322210, No. 62102403, No. 62136001 and No. 62088102), Beijing Municipal Natural Science Foundation for Distinguished Young Scholars (No. JQ21013), and Beijing Municipal Science and Technology Commission (No. Z231100005923031). We thank Yu Li from the High Performance Computing Center at Beijing Jiaotong University for his support and guidance in parallel computing optimization. We also thank Yu-Ying Yeh for generously sharing data for comparison.

References

[1] Sizhe An, Hongyi Xu, Yichun Shi, Guoxian Song, Umit Y. Ogras, and Linjie Luo. PanoHead: Geometry-aware 3D full-head synthesis in 360deg. In *IEEE/CVF Conference on Computer Vision and Pattern Recognition*, pages 20950–20959, 2023. 2

[2] Yunpeng Bai, Yanbo Fan, Xuan Wang, Yong Zhang, Jingxiang Sun, Chun Yuan, and Ying Shan. High-fidelity facial avatar reconstruction from monocular video with generative priors. In *IEEE/CVF Conference on Computer Vision and Pattern Recognition*, pages 4541–4551, 2023. 3

[3] Ananta R. Bhattacharai, Matthias Nießner, and Artem Sevestopolsky. TriPlaneNet: An encoder for EG3D inversion. *IEEE/CVF Winter Conference on Applications of Computer Vision*, 2024. 3

[4] V. Blanz and T. Vetter. A morphable model for the synthesis of 3D faces. In *Proceedings of ACM SIGGRAPH*, pages 187–194, 1999. 2

[5] Eric R Chan, Connor Z Lin, Matthew A Chan, Koki Nagano, Boxiao Pan, Shalini De Mello, Orazio Gallo, Leonidas J Guibas, Jonathan Tremblay, Sameh Khamis, et al. Efficient geometry-aware 3D generative adversarial networks. In *IEEE/CVF Conference on Computer Vision and Pattern Recognition*, pages 16123–16133, 2022. 2, 5, 6

[6] Sreenithy Chandran, Yannick Hold-Geoffroy, Kalyan Sunkavalli, Zhixin Shu, and Suren Jayasuriya. Temporally consistent relighting for portrait videos. In *IEEE/CVF Winter Conference on Applications of Computer Vision*, pages 719–728, 2022. 5

[7] Liang-Chieh Chen, George Papandreou, Florian Schroff, and Hartwig Adam. Rethinking atrous convolution for semantic image segmentation. *arXiv preprint arXiv:1706.05587*, 2017. 4

[8] Jia Deng, Wei Dong, Richard Socher, Li-Jia Li, Kai Li, and Li Fei-Fei. ImageNet: A large-scale hierarchical image database. In *IEEE/CVF Conference on Computer Vision and Pattern Recognition*, pages 248–255, 2009. 4

[9] Jiankang Deng, Jia Guo, Jing Yang, Niannan Xue, Irene Kotsia, and Stefanos Zafeiriou. ArcFace: Additive angular margin loss for deep face recognition. *IEEE Transactions on Pattern Analysis and Machine Intelligence*, 44(10):5962–5979, 2022. 5

[10] Yu Deng, Jiaolong Yang, Jianfeng Xiang, and Xin Tong. GRAM: Generative radiance manifolds for 3D-aware image generation. In *IEEE/CVF Conference on Computer Vision and Pattern Recognition*, 2022. 2

[11] Keyan Ding, Kede Ma, Shiqi Wang, and Eero P. Simoncelli. Image quality assessment: Unifying structure and texture similarity. *IEEE Transactions on Pattern Analysis and Machine Intelligence*, 44(5):2567–2581, 2022. 7

[12] Alexey Dosovitskiy, Lucas Beyer, Alexander Kolesnikov, Dirk Weissenborn, Xiaohua Zhai, Thomas Unterthiner, Mostafa Dehghani, Matthias Minderer, Georg Heigold, Sylvain Gelly, Jakob Uszkoreit, and Neil Houlsby. An image is worth 16x16 words: Transformers for image recognition at scale. *International Conference on Learning Representations*, 2021. 4

[13] Fan Fei, Yean Cheng, Yongjie Zhu, Qian Zheng, Si Li, Gang Pan, and Boxin Shi. SPLiT: Single portrait lighting estimation via a tetrad of face intrinsics. *IEEE Transactions on Pattern Analysis and Machine Intelligence*, 46(02):1079–1092, 2024. 2

[14] Yao Feng, Haiwen Feng, Michael J. Black, and Timo Bolkart. Learning an animatable detailed 3D face model from in-the-wild images. *ACM Transactions on Graphics*, 40(8), 2021. 2, 6, 7

[15] Anna Frühstück, Nikolaos Sarafianos, Yuanlu Xu, Peter Wonka, and Tony Tung. VIVE3D: Viewpoint-independent video editing using 3D-aware GANs. In *IEEE/CVF Conference on Computer Vision and Pattern Recognition*, 2023. 3

[16] Guy Gafni, Justus Thies, Michael Zollhöfer, and Matthias Nießner. Dynamic neural radiance fields for monocular 4D facial avatar reconstruction. In *IEEE/CVF Conference on Computer Vision and Pattern Recognition*, pages 8649–8658, 2021. 7

[17] Ian Goodfellow, Jean Pouget-Abadie, Mehdi Mirza, Bing Xu, David Warde-Farley, Sherjil Ozair, Aaron Courville, and Yoshua Bengio. Generative adversarial networks. *Communications of the ACM*, 63(11):139–144, 2020. 2

[18] Jonathan Ho, Ajay Jain, and Pieter Abbeel. Denoising diffusion probabilistic models. *Advances in Neural Information Processing Systems*, 33:6840–6851, 2020. 2

[19] Andrew Hou, Ze Zhang, Michel Sarkis, Ning Bi, Yiyi Tong, and Xiaoming Liu. Towards high fidelity face relighting with realistic shadows. In *IEEE/CVF Conference on Computer Vision and Pattern Recognition*, 2021. 2, 6, 7, 8

[20] Kaiwen Jiang, Shu-Yu Chen, Hongbo Fu, and Lin Gao. NeRFFaceLighting: Implicit and disentangled face lighting representation leveraging generative prior in neural radiance fields. *ACM Transactions on Graphics*, 42(3), 2023. 2, 3, 4, 5, 6, 7, 8

[21] Tero Karras, Samuli Laine, and Timo Aila. A style-based generator architecture for generative adversarial networks. In *IEEE/CVF Conference on Computer Vision and Pattern Recognition*, pages 4401–4410, 2019. 7

[22] Tero Karras, Samuli Laine, Miika Aittala, Janne Hellsten, Jaakko Lehtinen, and Timo Aila. Analyzing and improving the image quality of StyleGAN. In *IEEE/CVF Conference on Computer Vision and Pattern Recognition*, pages 8110–8119, 2020. 3, 4

[23] Diederik P Kingma and Jimmy Ba. Adam: A method for stochastic optimization. In *International Conference on Learning Representations*, 2015. 5

[24] Wei-Sheng Lai, Jia-Bin Huang, Oliver Wang, Eli Shechtman, Ersin Yumer, and Ming-Hsuan Yang. Learning blind video temporal consistency. In *European Conference on Computer Vision*, 2018. 4, 5

[25] Tianye Li, Timo Bolkart, Michael. J. Black, Hao Li, and Javier Romero. Learning a model of facial shape and expression from 4D scans. *ACM Transactions on Graphics*, 36 (6):194:1–194:17, 2017. 2

[26] Qiang Meng, Shichao Zhao, Zhida Huang, and Feng Zhou. MagFace: A universal representation for face recognition

and quality assessment. In *IEEE/CVF Conference on Computer Vision and Pattern Recognition*, 2021. 6

[27] Ben Mildenhall, Pratul P Srinivasan, Matthew Tancik, Jonathan T Barron, Ravi Ramamoorthi, and Ren Ng. NeRF: Representing scenes as neural radiance fields for view synthesis. *Communications of the ACM*, 65(1):99–106, 2021. 2

[28] Norman Müller, Yawar Siddiqui, Lorenzo Porzi, Samuel Rota Bulo, Peter Kortscheder, and Matthias Nießner. DiffRF: Rendering-guided 3D radiance field diffusion. In *IEEE/CVF Conference on Computer Vision and Pattern Recognition*, pages 4328–4338, 2023. 2

[29] Michael Niemeyer and Andreas Geiger. GIRAFFE: Representing scenes as compositional generative neural feature fields. In *IEEE/CVF Conference on Computer Vision and Pattern Recognition*, 2021.

[30] Xingang Pan, Xudong Xu, Chen Change Loy, Christian Theobalt, and Bo Dai. A shading-guided generative implicit model for shape-accurate 3D-aware image synthesis. In *Advances in Neural Information Processing Systems*, 2021. 2

[31] Rohit Pandey, Sergio Orts Escolano, Chloe Legendre, Christian Haene, Sofien Bouaziz, Christoph Rhemann, Paul Debevec, and Sean Fanello. Total Relighting: Learning to relight portraits for background replacement. *ACM Transactions on Graphics*, 40(4):1–21, 2021. 2, 7

[32] Foivos Paraperas Papantoniou, Alexandros Lattas, Stylianos Moschoglou, and Stefanos Zafeiriou. Relightify: Relightable 3D faces from a single image via diffusion models. In *International Conference on Computer Vision*, 2023. 2

[33] Haonan Qiu, Zhaoxi Chen, Yuming Jiang, Hang Zhou, Xiangyu Fan, Lei Yang, Wayne Wu, and Ziwei Liu. ReliTalk: Relightable talking portrait generation from a single video. In *International Journal of Computer Vision*, 2024. 2, 6, 8

[34] Ravi Ramamoorthi and Pat Hanrahan. An efficient representation for irradiance environment maps. In *Proceedings of the 28th Annual Conference on Computer Graphics and Interactive Techniques*, page 497–500, 2001. 3

[35] Anurag Ranjan, Kwang Moo Yi, Rick Chang, and Oncel Tuzel. FaceLit: Neural 3D relightable faces. In *IEEE/CVF Conference on Computer Vision and Pattern Recognition*, 2023. 2

[36] Daniel Roich, Ron Mokady, Amit H Bermano, and Daniel Cohen-Or. Pivotal tuning for latent-based editing of real images. *ACM Transactions on Graphics*, 42(1):1–13, 2022. 3, 6

[37] Katja Schwarz, Yiyi Liao, Michael Niemeyer, and Andreas Geiger. GRAF: Generative radiance fields for 3D-aware image synthesis. In *Advances in Neural Information Processing Systems*, 2020. 2

[38] Jingxiang Sun, Xuan Wang, Yichun Shi, Lizhen Wang, Jue Wang, and Yebin Liu. IDE-3D: Interactive disentangled editing for high-resolution 3D-aware portrait synthesis. *ACM Transactions on Graphics*, 41(6):1–10, 2022.

[39] Jingxiang Sun, Xuan Wang, Lizhen Wang, Xiaoyu Li, Yong Zhang, Hongwen Zhang, and Yebin Liu. Next3D: Generative neural texture rasterization for 3D-aware head avatars. In *IEEE/CVF Conference on Computer Vision and Pattern Recognition*, 2023. 2

[40] Jia-Mu Sun, Wu Tong, and Lin Gao. Recent advances in implicit representation based 3D shape generation. *Visual Intelligence*, 2, 2024. 2

[41] Zachary Teed and Jia Deng. RAFT: Recurrent all-pairs field transforms for optical flow. In *European Conference on Computer Vision*, pages 402–419, 2020. 6

[42] Ayush Tewari, Michael Zollhofer, Hyeongwoo Kim, Pablo Garrido, Florian Bernard, Patrick Perez, and Christian Theobalt. MoFA: Model-based deep convolutional face autoencoder for unsupervised monocular reconstruction. In *International Conference on Computer Vision Workshops*, pages 1274–1283, 2017. 2

[43] Omer Tov, Yuval Alaluf, Yotam Nitzan, Or Patashnik, and Daniel Cohen-Or. Designing an encoder for StyleGAN image manipulation. *ACM Transactions on Graphics*, 40(4), 2021. 3

[44] Alex Trevithick, Matthew Chan, Michael Stengel, Eric R. Chan, Chao Liu, Zhiding Yu, Sameh Khamis, Manmohan Chandraker, Ravi Ramamoorthi, and Koki Nagano. Real-time radiance fields for single-image portrait view synthesis. In *ACM Transactions on Graphics*, 2023. 3, 4, 7

[45] Tengfei Wang, Bo Zhang, Ting Zhang, Shuyang Gu, Jianmin Bao, Tadas Baltrusaitis, Jingjing Shen, Dong Chen, Fang Wen, Qifeng Chen, et al. RODIN: A generative model for sculpting 3D digital avatars using diffusion. In *IEEE/CVF Conference on Computer Vision and Pattern Recognition*, pages 4563–4573, 2023. 2

[46] Zhibo Wang, Xin Yu, Ming Lu, Quan Wang, Chen Qian, and Feng Xu. Single image portrait relighting via explicit multiple reflectance channel modeling. *ACM Transactions on Graphics*, 39(6):1–13, 2020. 7

[47] Jiaxin Xie, Hao Ouyang, Jingtang Piao, Chenyang Lei, and Qifeng Chen. High-fidelity 3D GAN inversion by pseudo-multi-view optimization. 2023. 3

[48] Eric Zhongcong Xu, Jianfeng Zhang, Junhao Liew, Wenqing Zhang, Song Bai, Jiashi Feng, and Mike Zheng Shou. PV3D: A 3D generative model for portrait video generation. In *International Conference on Learning Representations*, 2023. 5

[49] Yang Xue, Yuheng Li, Krishna Kumar Singh, and Yong Jae Lee. Giraffe hd: A high-resolution 3d-aware generative model. In *IEEE/CVF Conference on Computer Vision and Pattern Recognition*, 2022. 2

[50] Yu-Ying Yeh, Koki Nagano, Sameh Khamis, Jan Kautz, Ming-Yu Liu, and Ting-Chun Wang. Learning to relight portrait images via a virtual light stage and synthetic-to-real adaptation. *ACM Transactions on Graphics*, 2022. 2, 7

[51] Fei Yin, Yong Zhang, Xuan Wang, Tengfei Wang, Xiaoyu Li, Yuan Gong, Yanbo Fan, Xiaodong Cun, Öztireli Cengiz, and Yujiu Yang. 3D GAN inversion with facial symmetry prior. In *IEEE/CVF Conference on Computer Vision and Pattern Recognition*, 2023. 3

[52] Yu Yin, Kamran Ghasedi, HsiangTao Wu, Jiaolong Yang, Xin Tong, and Yun Fu. NeRFInvertor: High fidelity NeRF-GAN inversion for single-shot real image animation. In *IEEE/CVF Conference on Computer Vision and Pattern Recognition*, pages 8539–8548, 2023. 3

- [53] Ziyang Yuan, Yiming Zhu, Yu Li, Hongyu Liu, and Chun Yuan. Make encoder great again in 3D GAN inversion through geometry and occlusion-aware encoding. In *International Conference on Computer Vision*, 2023. [3](#)
- [54] Longwen Zhang, Qixuan Zhang, Minye Wu, Jingyi Yu, and Lan Xu. Neural video portrait relighting in real-time via consistency modeling. In *International Conference on Computer Vision*, pages 802–812, 2021. [2](#), [7](#)
- [55] Richard Zhang, Phillip Isola, Alexei A Efros, Eli Shechtman, and Oliver Wang. The unreasonable effectiveness of deep features as a perceptual metric. In *IEEE/CVF Conference on Computer Vision and Pattern Recognition*, 2018. [4](#), [5](#), [7](#)
- [56] Hao Zhou, Sunil Hadap, Kalyan Sunkavalli, and David W. Jacobs. Deep single portrait image relighting. In *Proceedings of the IEEE/CVF International Conference on Computer Vision*, 2019. [2](#), [5](#), [6](#), [7](#), [8](#)
- [57] Hao Zhou, Sunil Hadap, Kalyan Sunkavalli, and David W Jacobs. Deep single-image portrait relighting. In *IEEE/CVF Conference on Computer Vision and Pattern Recognition*, pages 7194–7202, 2019. [2](#)
- [58] Wojciech Zienonka, Timo Bolkart, and Justus Thies. Instant volumetric head avatars. In *IEEE/CVF Conference on Computer Vision and Pattern Recognition*, pages 4574–4584, 2023. [5](#), [6](#), [7](#), [8](#)